

Current Biology, Volume 24

Supplemental Information

Representation of Object Weight

in Human Ventral Visual Cortex

Jason P. Gallivan, Jonathan S. Cant, Melvyn A. Goodale, and J. Randall Flanagan

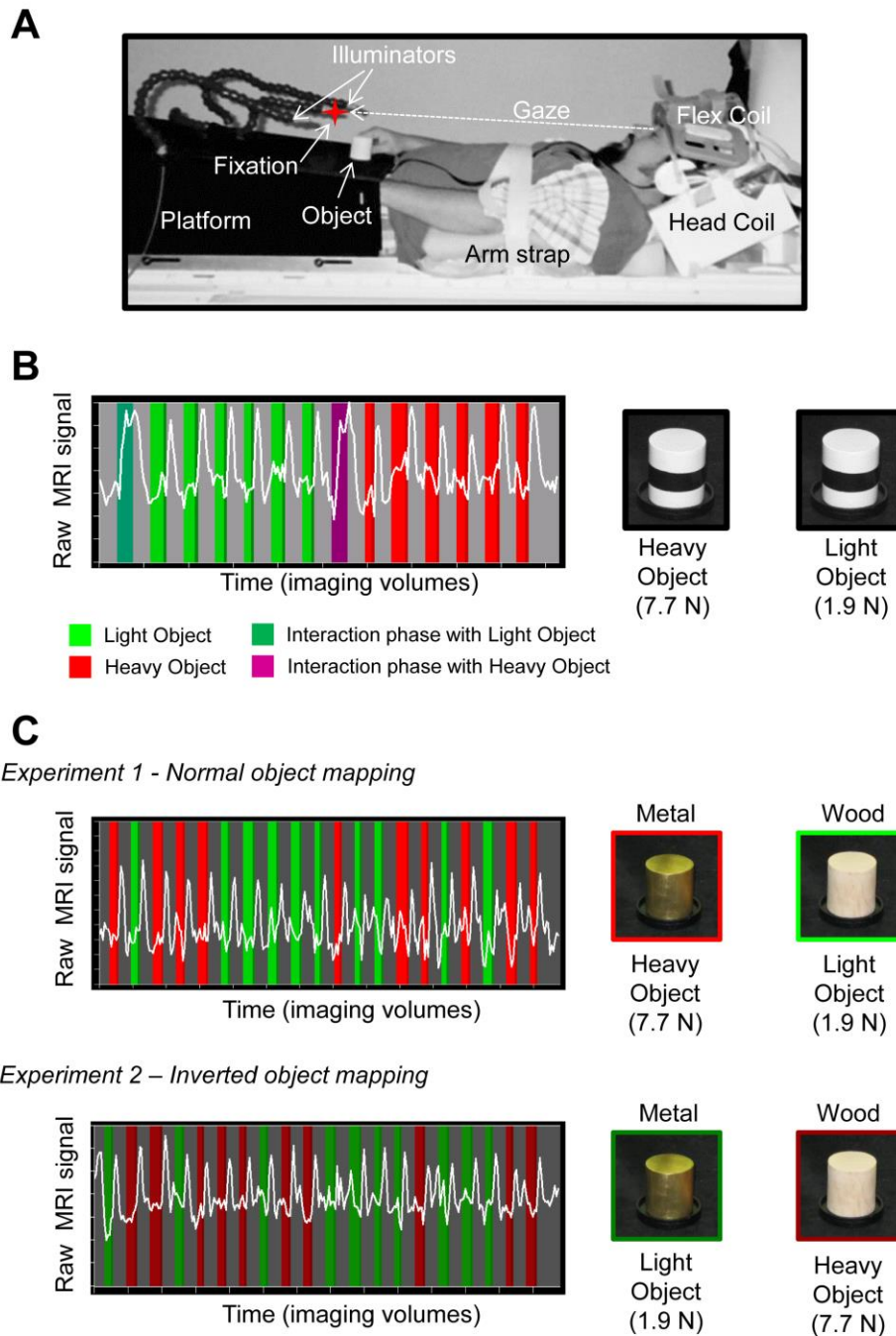


Figure S1, Related to Figure 1: Subject setup and experimental protocols. **A)** Subject setup shown from side view. **B)** Study 1 example protocol for a single experimental fMRI run (left) and objects used (right). White trace (at left) is the raw MRI BOLD response taken from the motor cortex of a representative subject. **C)** Study 2 example protocols for single experimental fMRI runs belonging to the first (top left) and second (bottom left) experiments and the corresponding set of objects used (top and bottom right, respectively). White traces (at left) are the raw MRI BOLD responses taken from the motor cortex of the same subject shown in B.

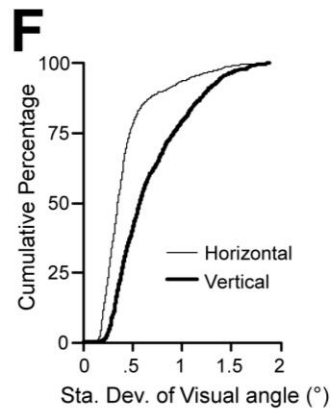
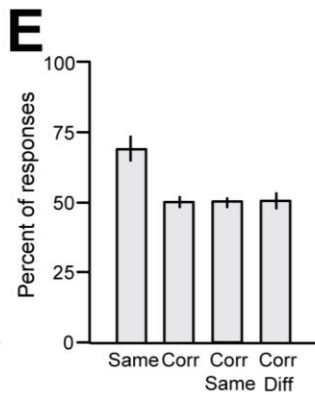
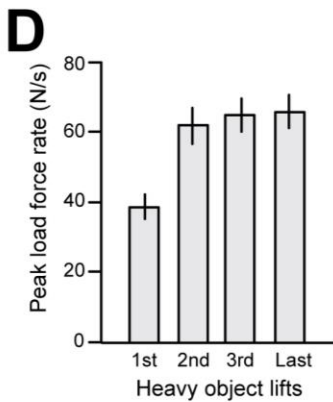
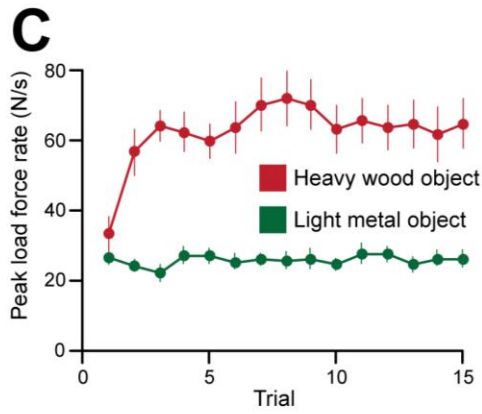
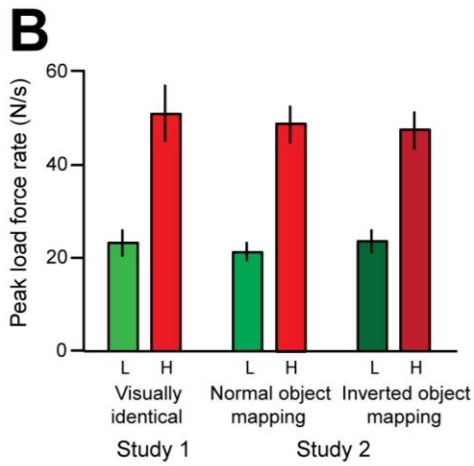
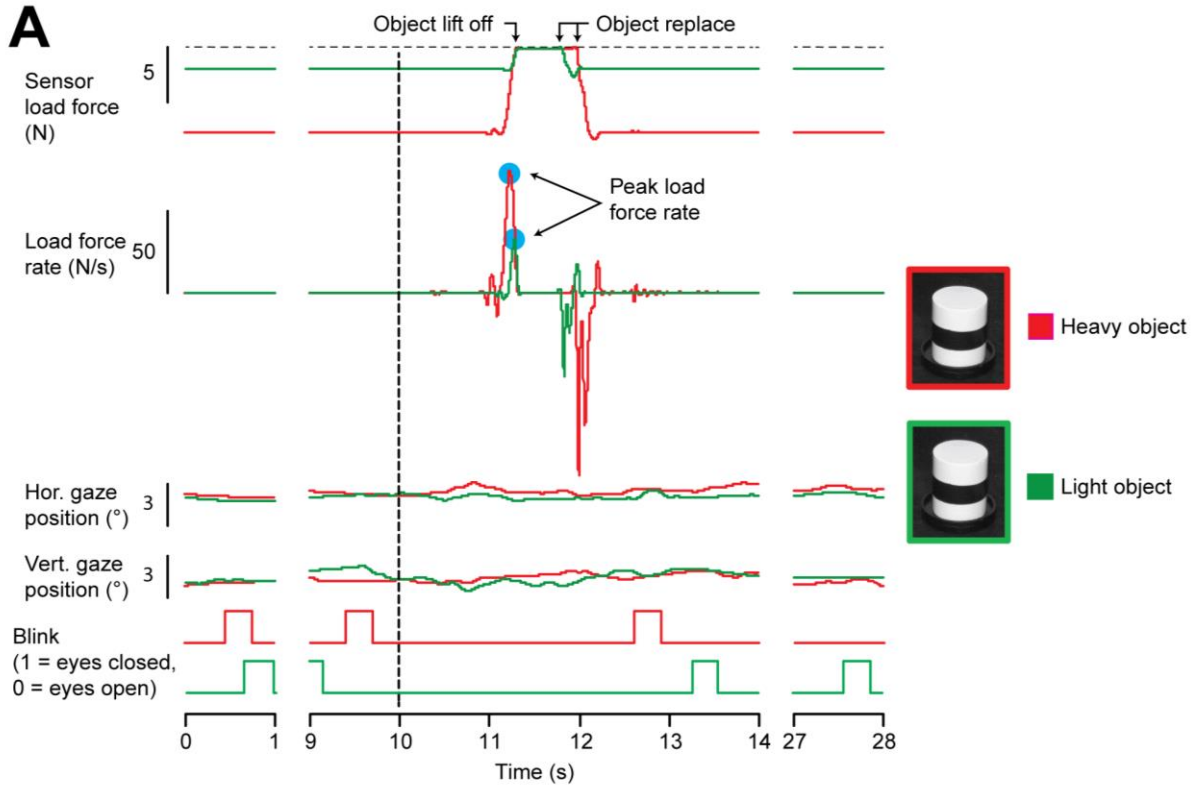
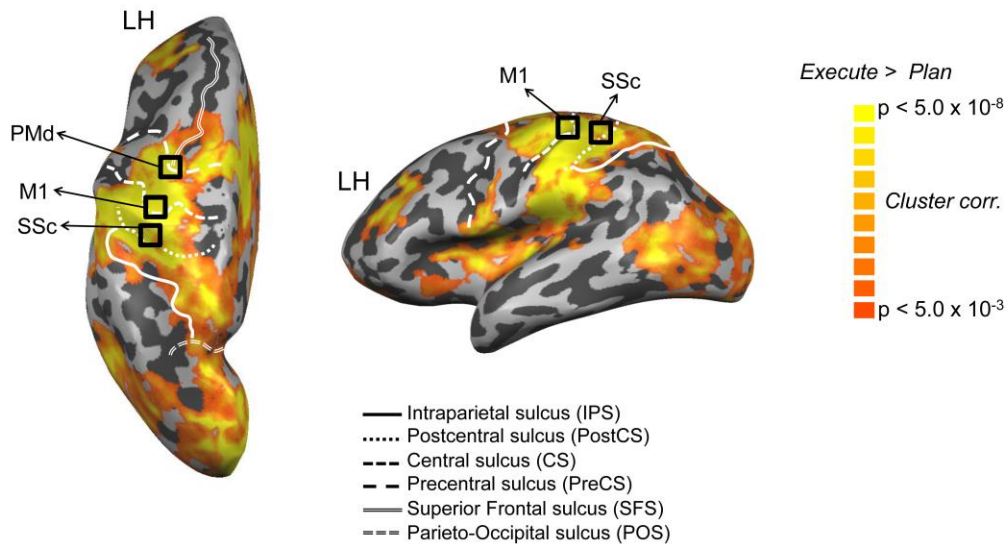


Figure S2, Related to Figure 2: Behavioural Results. **A)** Load force, load force rate, horizontal and vertical gaze positions, and blink state for two event-related delayed lift trials with the heavy (red traces) or light (green traces) objects used in Study 1, shown for one representative subject. Note that only the first and last seconds and the period between 9 and 14 seconds of each trial are shown. The vertical dashed line indicates the time of the Go signal to execute the lift. The horizontal dashed line represents 0 N, which occurred when the object was lifted off the force sensor. The blue circles denote the initial peak load force rates in the two lifts. **B)** Mean peak load force rate, based on participant averages, when lifting the light (L) and heavy (H) visually identical objects (used in Study 1) and the normal and inverted texture-weight objects (used in Study 2). In all cases, peak load force rate was greater for the heavy object, indicating that participants predicted the object weights when lifting (and held in memory over the delay period of each trial the weight of the object to be lifted). **C)** Mean peak load force rate, averaged across participants, during the 15 alternated lifts of each inverted texture-weight object (during the 'learning phase' when subjects learned the new association between object weight and texture). Note that participants increased load force more rapidly for the heavy wood object, in comparison to the light metal object, from the second lift of each object onwards, indicating that they quickly learned the weights of the objects. **D)** Mean peak load force rate, based on participant means, for the first, second, third and last lifts of the heavy object in the control experiment for Study 1 in which participants lifted the light and heavy objects in alternating blocks of 7 ± 2 trials. The peak load force rate was far smaller on the first lift, indicating that participants could not predict using visual cues when the light object was replaced by the similar looking heavy object. [Note that we focused on lifts of the heavy object because the initial peak load force rate cannot be accurately measured prior to lift-off on first lifts of the light object following a block of trials of heavy objects [S1]]. **E)** Results of the perceptual discrimination task in which participants reported, via key press responses, whether the object presented on the current trial was the same as or different than the object presented on the previous trial (i.e., one-back task). On average participants judged the object to be the 'same' on 69.3 % of trials (Same) but were correct (Corr) on 50.2 % of trials. Similar percentages of correct responses were observed regardless of whether participants judged the object to be the same (49.8 %; Corr Same) or different (51.1 %; Corr Diff). These results indicate that participants could not perceptually discriminate between the visually similar heavy and light objects used in Study 1. **F)** Cumulative distributions of the standard deviation of horizontal and vertical gaze positions in all lift trials performed by all participants in both behavioural experiments. The results, in combination with our observations during analysis that participants did not make saccades during these trials, demonstrates that participants were able to successfully maintain gaze at the fixation point, as instructed by the experimenter. In all plots, error bars represent ± 1 SEM.

A Somatomotor Regions



B Occipitotemporal Regions

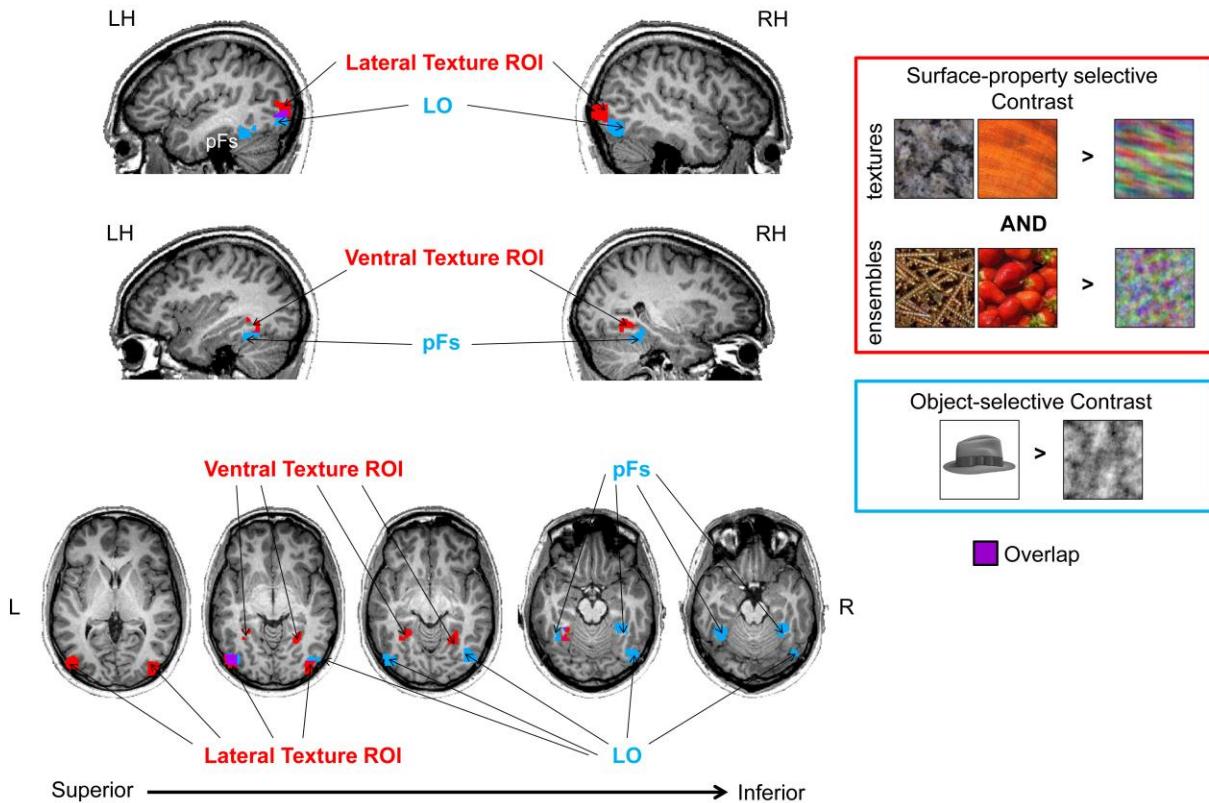


Figure S3, Related to Figure 3: ROI Locations in a representative subject. A) Somatomotor control areas examined with fMRI decoding methods. Cortical areas that exhibited larger responses during movement generation than planning [Execute > Plan] are shown in

orange/yellow activation on the inflated hemisphere of a representative subject. Sulcal landmarks are denoted by white lines (stylized according to the corresponding legend). The selected ROIs are bordered in black. **B)** Occipitotemporal category-selective ROIs (at $t = 3$, $p < 0.005$, corrected) overlaid on the transverse and sagittal anatomical slices of the same subject as in A. Blue (object-selective) ROIs were defined by the contrast of Objects > Scrambled (see right). Red (object texture-sensitive) ROIs were defined by the conjunction contrast of Object Ensembles > phase-scrambled versions of these images AND Object Textures > phase-scrambled versions of these images (see right). Small regions of overlap between the object- and texture-sensitive ROIs are shown in purple. L = left; R = right; LH = left hemisphere; RH = right hemisphere; corr. = corrected.

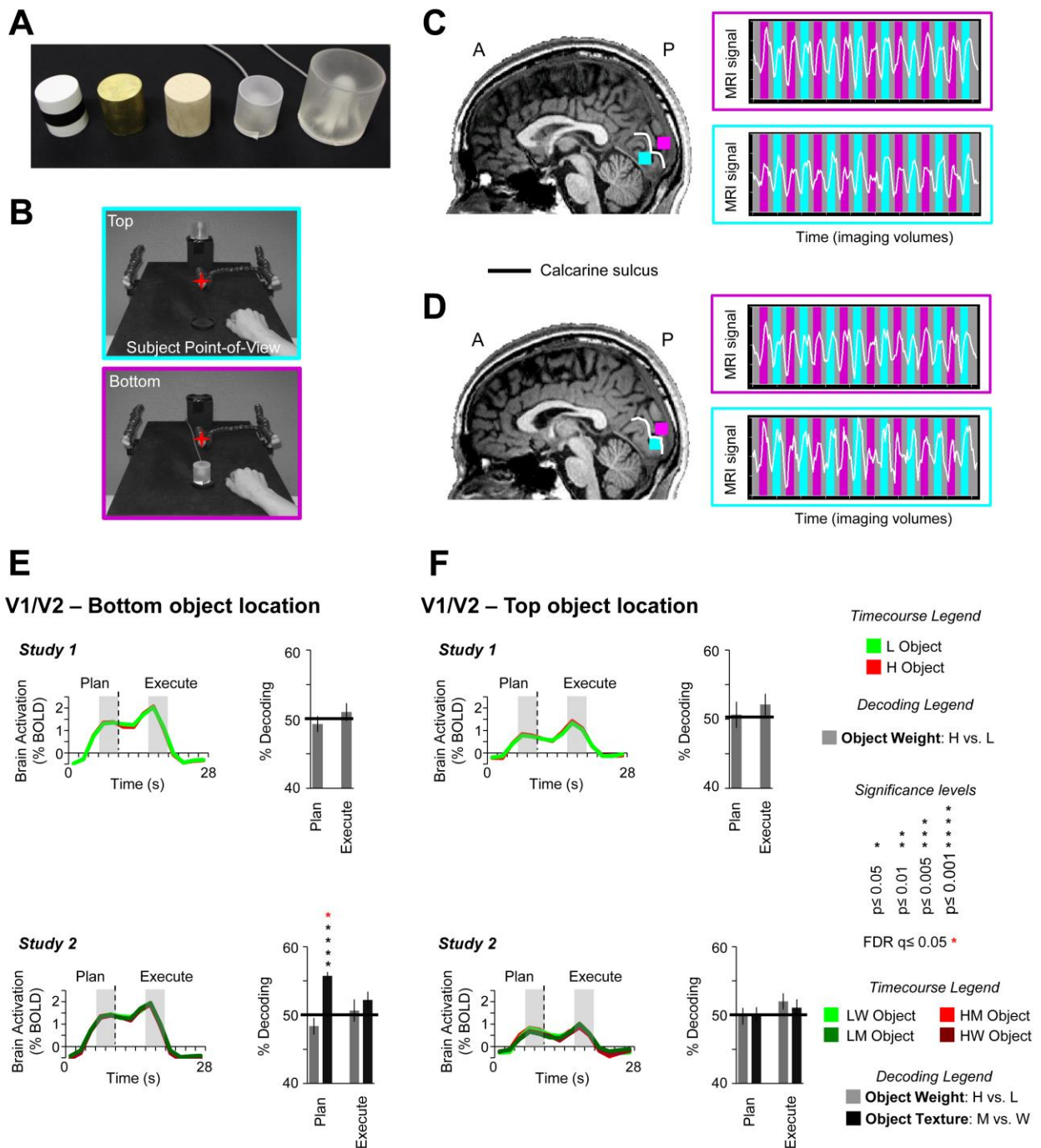


Figure S4, Related to Figure 4: Methods for retinotopically mapping object locations and corresponding decoding results for Study 1 and 2. A) Different objects used in Studies 1 and 2 and corresponding illuminable objects. B) Experimental setup for retinotopic mapping of two object locations (Bottom object was positioned in the same location as the target object(s) used in Studies 1 and 2 and the Top object was positioned in a location not acted upon during the

experiments). Bottom and Top illuminable objects correspond to the illuminable objects shown in A (second and first from the right, respectively). Note that the Top object location was retinotopically mapped as a control ROI; if decoding is found in V1/V2, then it should be specific to the retinotopic representation of the target (Bottom) but not control (Top) object location. **C)** Left, Cortical representation in V1/V2 for a representative subject in Study 1 of example object locations shown in B (pink ROI is based on contrast of Bottom > ITI; cyan ROI is based on contrast of Top > ITI). Right, example protocol for a single experimental fMRI run of the retinotopic object mapping localizer. White traces are the raw MRI BOLD responses taken from the two V1/V2 regions at left (border colours denote ROI). **D)** Same format and subject as in C, but shows the cortical representation in V1/V2 for Study 2 object positions. Note that data from C and D are from separate testing sessions (Studies 1 and 2), thus accounting for small differences in retinotopic location. **E-F)** Percentage signal change time courses and decoding accuracies in Study 1 and 2 for the Bottom and Top object locations, plotted and computed the same as in Figure 2.

Mean ROI sizes across subjects (N=13)

Brain Areas	mm³	voxels
<i>Occipitotemporal ROIs</i>		
<u>Object-sensitive areas</u>		
L-LO	1906.5	70.6
R-LO	1803.7	66.8
L-pFs	1258.8	46.6
R-pFs	1098.1	40.7
<u>Texture-sensitive areas</u>		
L-Lateral region	1557.4	57.7
R-Lateral region	1660.1	61.5
L-Ventral region	894.4	33.1
R-Ventral region	1160.2	43
<i>Somatomotor ROIs</i>		
SSc	2530.5	93.7
M1	2695.8	99.8
PMd	2523	93.4
<i>Object Mapping-defined Visual Cortex Regions</i>		
<u>Study 1</u>		
V1/V2 Bottom Location (above calcarine sulcus)	982.9	36.4
V1/V2 Top Location (below calcarine sulcus)	975.4	36.1
<u>Study 2</u>		
V1/V2 Bottom Location (above calcarine sulcus)	934.5	34.6
V1/V2 Top Location (below calcarine sulcus)	885.1	32.8

Table S1, Related to Figure 2: Mean ROI sizes across subjects from ACPC-aligned data (in mm³ and functional voxels).

Comparisons	No. of Subjects	% Object ROIs	SEM
L-LO and L-Lateral region	11	11	3.3
R-LO and R-Lateral region	8	14.5	4.2
L-pFs and L-Ventromedial region	8	25	5.8
R-pFs and R-Ventromedial region	6	29.5	9.5

Table S2, Related to Figure 4: Mean voxel overlap between the localizer-defined Object- and Texture-sensitive ROIs. No. of Subjects denotes the number of subjects in which the corresponding ROIs showed overlap. % Object ROIs denotes the percentage of total object-sensitive voxels (either LO or pFs) that overlapped with the texture-sensitive ROIs.

SUPPLEMENTAL EXPERIMENTAL PROCEDURES

Participants

Thirteen right-handed volunteers (6 females; mean age: 24.2 years, age range: 20-28), as assessed by the Edinburgh handedness questionnaire [S2], participated in three separate fMRI testing sessions and two separate behavioural testing sessions, all performed within a 10 month period. The testing order for each subject was as follows: Behavioural testing session 1, fMRI testing session for Study 1, fMRI Localizer session, fMRI testing session for Study 2, and Behavioural testing session 2. The total MRI testing time per subject was ~ 8.5 hours and the total behavioural testing time per subject was ~ 3 hours. Informed consent and consent to publish was obtained in accordance with ethical standards set out by the Declaration of Helsinki (1964) and with procedures approved by Queen's University's Health Sciences Research Ethics Board. Subjects were naïve with respect to hypothesis testing.

Object Lifting Experiments: fMRI Setup and Apparatus

Each subject's workspace consisted of a black platform placed over the waist and tilted away from the horizontal at an angle (~15°) to maximize comfort and target visibility. To facilitate direct viewing of the workspace, we also tilted the head coil (~20°) and used foam cushions to give an approximate overall head tilt of 30° (see Fig. S1A). For each trial, participants prepared and then executed individual grasp-and-lift movements with their right hand upon a single centrally located cylindrical target object [5 x 5.5 cm (radius x height)], which could be one of two different weights: 7.7 N (Heavy) or 1.9 N (Light). For the execution phase of the trial, subjects were required to precision grasp-and-then-lift the object with their thumb and index finger (~2 cm above the platform, via a rotation of the wrist), hold it in midair for 1 s, and then replace it. Participants were instructed to keep the timing of each hand action as similar as possible. Following the completion of each trial, the target object was replaced by the experimenter. The exact placement of the target object on the platform was adjusted to match each participant's arm length such that all required grasp-and-lift actions were comfortable and ensuring that only movement of the forearm, wrist and fingers were required. To mark the position of the target object, the object was placed within reach by the participant's right hand at a central position on the platform, in line with the point of fixation. Then, to maintain trial-to-trial consistency with respect to this object position throughout the full length of the experiment (and aid the experimenter in replacing the object in the dark in between trials), a custom-made black disk with raised edges [7 x 1 cm (radius x height) with a 0.5 cm lip of 0.7 cm thickness] was secured to the platform at this desired location.

During the experiment, the target object was illuminated from the side by two bright white Light Emitting Diodes (LEDs) attached to flexible plastic stalks (Loc-Line, Lockwood Products, Lake Oswego, OR), positioned to the left and right of the subject (see Fig. 1B). During participant setup, both illuminator LEDs were positioned so as to brightly illuminate the target object. Experimental timing and lighting were controlled with in-house software created with MATLAB (The Mathworks, Natick, MA). To control for eye movements, a small red fixation LED (attached to a flexible plastic stalk) was placed above and at a slightly further depth location (~5 cm) than the pre-specified target position and subjects were required to always foveate this

fixation LED during fMRI data collection (the fixation point was ~100 cm from the participants' eyes and at a visual angle of ~15° above the participants' natural line of gaze).

fMRI Study 1 Details

The differently weighted target objects of Study 1 were visually identical and painted white to increase their contrast with the background (a black strip of tape was placed around their centres to provide a target zone for participants to grip the object). The repeated nature of the trial sequence following each Interaction phase (see Fig. S1B) allowed participants to fully predict the weight of the object to be lifted on each event-related trial. Each trial was made up of a 6-12 s Plan epoch, a 2-s Execute epoch, and a 16-s ITI (24-30 s total duration; see below for further details). Each experimental run lasted 6 min 56 sec and was composed of six consecutive event-related trials per object weight (heavy or light) with each of these sequences being preceded by an Interaction phase with that same object (see Fig. S1B). In each Interaction phase, to learn the weight of the object, participants lifted the centrally located object six successive times, each lift spaced 2-s apart (each lift was cued with its own auditory 'beep'). The onset of each Interaction phase was cued via the auditory command "Interact" that was played concurrently as the subject's workspace was illuminated. Following the completion of each Interaction phase (14 s total duration), the illuminators were extinguished, and subjects then waited in the dark while maintaining fixation for 16 s, prior to the first event-related trial of the predictable event-related trial sequence beginning. The ordering of the two trial types (heavy or light object) were alternated across runs and balanced across subjects. Subjects participated in 8-12 experimental runs of this object-lifting task.

fMRI Study 2 Details

In the first experiment of Study 2 subjects acted upon objects with stereotypical object weight and texture associations (i.e., metal heavy object and wood light object). In the second experiment of Study 2 subjects acted upon visually identical objects but with the inverse associations (i.e., wood heavy object and metal light object). Thus, while on each trial in each experiment subjects could reliably predict the weight of the object to be lifted based on visual cues alone, across the whole of the study, object weight could be decoupled from the object texture that cued weight. Like Study 1, each trial in Expt. 1 and 2 of Study 2 was made up of a 6-12 s Plan epoch, a 2-s Execute epoch, and a 16-s ITI (24-30 s total duration; see below for further details). Each experimental run lasted 9 min 20 sec and the two trial types (heavy or light object), with ten repetitions per condition (20 trial total), were randomized within a run and balanced within each experiment so that each trial type was preceded and followed equally often by every other trial type. Prior to beginning MRI scanning for both the first and second experiments of the study, subjects learned the associations between object weight and texture by lifting each object 15 times in an alternating fashion (lifts spaced approximately 2 s apart at their own pace). Subjects participated in 8-10 experimental runs of this object-lifting task (4-5 each of Expt. 1 and 2).

Object Lifting Experiments: fMRI Design and Timing

For both Study 1 and 2, we used a jittered slow event-related delay paradigm in which the planning of hand actions was separated in time from their execution (see Fig. 1A). This design allowed us to isolate the preparatory neural processes that evolve prior to movement onset while avoiding many of the potential sensory confounds that arise during the hand movement itself

(e.g., visual stimulation created by the hand moving, somatosensory stimulation created by the hand contacting and lifting the object, etc.). We adapted this paradigm from previous work with eye- and arm-movements that have successfully isolated delay period activity from the transient neural responses following the onset of movement [S3-7] and, in some of our previous work, we have successfully used the spatial voxel patterns of delay period responses in various brain regions to predict different upcoming movements directed towards objects [S8-12].

In each study, each trial began with the Plan epoch, in which, concurrently, the subject's workspace was illuminated (revealing the centrally located target object) and the auditory cue, "Ready", was delivered via headphones. Following a jittered delay interval (6-12 s), a 0.5-s auditory 'beep' cued participants to immediately execute the grasp-and-lift action, initiating the Execute epoch of the trial. Two seconds following the beginning of this auditory Go cue, the illuminator was turned off, providing the cue for subjects to return their hand to its peripheral starting position. After the illuminator was extinguished, subjects then waited in the dark while maintaining fixation for 16 s, allowing the BOLD response to return to baseline prior to the next trial (ITI phase). Other than the execution of these grasp-and-lift actions, throughout all other phases of the trial (Plan epoch and ITI) subjects were instructed to keep their hand still (in a relaxed fist) and in a pre-specified 'home' position on the right surface of the platform (see Fig. 1B). For each participant the home/starting position was marked with an elevated small black plastic capsule taped to the surface of the platform and subjects were required to always return to this same position following execution of the hand movement. Importantly, within a full testing session, the target object never changed its centrally located position, thus eliminating retinal differences across trial types.

Separate practice sessions were carried out before the actual experiment to familiarize participants with the delayed timing of the task. One of these sessions was before participants entered the scanner (see Behavioural testing session 1 below) and another was during the anatomical scan (collected at the beginning of every experiment). An fMRI testing session for each participant included set-up time (~45 minutes), one anatomical scan, eight to twelve experimental runs (this varied from 10-12 runs for Study 1 and between 8 and 10 runs for Study 2), two to three Object Mapping localizer scans (see paragraph below), and lasted approximately 3 hours. Throughout the experiment, the subject's hand movements were monitored using an MR-compatible infrared-sensitive camera (MRC Systems GmbH, Heidelberg, Germany), optimally positioned on one side of the platform and facing towards the subject. The videos captured during the experiment were analyzed off-line to verify that the subjects were performing the task as instructed. In scanner eye-tracking could not be performed because our eye-tracking software does not work while the head is tilted due to a partial occlusion from the eyelids.

Retinotopic mapping of object locations ('Object-mapping')

To retinotopically map the location of the target object in Studies 1 and 2, at the end of each testing session, hollow semi-opaque illuminable objects (containing two super-bright LEDs at their center, which could flicker in an on-off fashion at 5Hz) were presented in 1) a location at which the target object appeared throughout the object lifting experiments (lower-visual field, Bottom position), and 2) a location outside of reach (~30 cm further than the fixation LED; ~130 cm from participants' eyes) that was never acted upon throughout the experiment (upper-visual

field, Top position). The Bottom position illuminable object was of the same size and shape as that used in the corresponding object lifting experiments (see Fig. S4A). The Top position object was of larger size [8 x 8.5 cm (radius x height)], subtending an approximately similar visual field angle as that of the Bottom position object (Bottom position object, $\sim 3.3^\circ$; Top position object, $\sim 3.7^\circ$; see Fig. S4A). To ensure that the retinotopic location of the Top object was fully above the horizontal plane of fixation (from the participant's point-of-view), it was placed upon a black wooden block [11.5 x 11.5 x 12 cm (width x length x height); see Fig. S4B). Each experimental run lasted 6 min 16 sec and was composed of eight stimulus epochs per object location (12 s each), with each stimulus block separated by an ITI (10 s each, in which subjects simply maintained fixation in the dark), and two baseline epochs (12 s each; also fixation in dark) placed at the beginning and end of each run (see Fig. S4C, D for protocols). All subjects participated in two or three of these 'object mapping' localizer scans, conducted at the very end of both Study 1 and 2 testing sessions.

Localizer Experiments

In a separate testing session, each subject participated in three types of functional localizer runs. The first included stimulus blocks of black-and-white photographs consisting of faces, scenes, objects, and phase scrambled versions of these stimuli (from [S13]) and was used to localize object-sensitive areas of cortex. The second included stimulus blocks of colour photographs consisting of object ensembles and surface textures and phase scrambled versions of these stimuli (also from [S13]) and was used to identify areas sensitive to the viewing of object texture. The last included standard retinotopy localizer stimuli (rotating wedges and contracting rings, see [S14-16] for details) and was used to demarcate the boundaries of early visual areas. In addition to these localizers, we also collected a high-resolution anatomical image from each of the participating subjects. All stimuli were rear-projected with an LCD projector (NEC LT265 DLP projector; resolution, 1024 x 768; 60 Hz refresh rate) onto a screen mounted behind the subject. The subject viewed the images through a mirror mounted to the head coil directly above the eyes.

Object- and Texture-sensitive Localizers

In the object-sensitive localizer, used to identify areas LO and pFs, each run consisted of four blocks each of faces, scenes, intact objects, and phase-scrambled objects. Each stimulus block was 16 s long and contained 20 different images, each presented for 750 ms, and followed by a 50 ms blank period. Periods of fixation (8 s each) were presented at the beginning, middle, and end of a run. In the texture-sensitive localizer, used to identify texture-selective areas in lateral occipital cortex and ventromedial cortex [S13], each run consisted of four blocks each of intact object ensembles, intact object textures, and their phase-scrambled counterparts (consisting of full-color object ensembles and surface textures, with each category containing equal numbers of living and non-living stimuli). All other aspects of this localizer were identical to that of the object-sensitive localizer, with the exception that each image in a block was presented for 500 ms and was followed by a 300 ms blank period. In both types of localizer scans, participants were required to maintain fixation on a dot (small red circle) superimposed on the center of each image. To encourage participants to maintain attention during the scans, subjects performed a detection task throughout, whereby responses were made, via a right-handed button press, whenever they detected a slight spatial jitter, occurring randomly in 1 out of every 10 images. For each localizer, there were two unique run orders, and no images were repeated in a given

run. All images subtended $12.5^\circ \times 12.5^\circ$ of visual angle. Each run lasted 4 min 40 s. All subjects participated in three of each object- and texture-sensitive localizer runs.

Retinotopic mapping of early visual areas

Early visual areas (i.e., V1, V2, and V3) were mapped and delineated using standard phase-encoded protocols and retinotopic mapping procedures [S17-19]. Subjects maintained fixation while viewing ‘traveling wave’ stimuli consisting of rotating wedges and expanding rings. Rotating wedge and expanding ring stimuli were presented in separate scans (each scan was 12 min in duration). To encourage participants to maintain attention during the retinotopy scans, subjects performed a detection task throughout, whereby responses were made, via a right-handed button press, whenever they detected a slight dimming of the fixation point (this occurred on average every 4.5 s). Cross-correlation analyses were used to construct phase-encoded retinotopic maps of polar angle and eccentricity and early visual area boundaries were delineated using field-sign mapping procedures [S18].

MRI acquisition and preprocessing

Subjects were scanned using a 3-Tesla Siemens TIM MAGNETOM Trio MRI scanner located at the Centre for Neuroscience Studies in Queen’s University (Kingston, Ontario, Canada). The T1-weighted anatomical image was collected using an ADNI MPRAGE sequence (TR = 1760 ms, TE = 2.98 ms, field of view = 192 mm x 240 mm x 256 mm, matrix size = 192 x 240 x 256, flip angle = 9° , 1 mm isotropic voxels). Functional MRI volumes were collected using a T2*-weighted single-shot gradient-echo echo-planar imaging (EPI) acquisition sequence (time to repetition (TR) = 2000 ms, slice thickness = 3 mm, in-plane resolution = 3 mm x 3 mm, time to echo (TE) = 30 ms, field of view = 240 mm x 240 mm, matrix size = 80 x 80, flip angle = 90° , and acceleration factor (integrated parallel acquisition technologies, iPAT) = 2 with generalized auto-calibrating partially parallel acquisitions (GRAPPA) reconstruction). Each volume comprised 35 contiguous (no gap) oblique slices acquired at a $\sim 30^\circ$ caudal tilt with respect to the plane of the anterior and posterior commissure (AC-PC), providing near whole brain coverage. In Studies 1 and 2, we used a combination of imaging coils to achieve a good signal:noise ratio and to enable direct object viewing without mirrors or occlusion. Specifically, we tilted ($\sim 20^\circ$ degrees) the posterior half of the 12-channel receive-only head coil (6-channels) and suspended a 4-channel receive-only flex coil over the anterior-superior part of the head. In the Localizer session, subjects were scanned using a conventional setup (i.e., stimuli back-projected onto a 2-D screen and viewed through a mirror), with a 12-channel receive-only head coil. The cortical surface for each subject was reconstructed from a high-resolution anatomical image, a procedure that included segmenting the gray and white matter and inflating the boundary surface between them. For analyses, all data (from Studies 1 and 2 and the Localizer experiments) were spatially aligned to the corresponding individual’s high-resolution anatomical image collected during the Localizer experiment testing session. All preprocessing and univariate analyses were performed using Brain Voyager QX version 2.6 (Brain Innovation, Maastricht, Netherlands).

Following slice scan-time correction, 3D motion correction (such that each volume was aligned to the volume of the functional scan closest in time to the anatomical scan), high-pass temporal filtering (filtering was adjusted based on condition frequency; Studies 1 and 2: 4 cycles/run; Object mapping runs: 5 cycles/run; Object- and Texture-sensitive runs: 3 cycles/run; Retinotopy runs: 5 cycles/run) and functional-to-anatomical co-registration, functional and anatomical

images were rotated such that the axial plane passed through the anterior and posterior commissures (AC-PC space). Other than the sinc interpolation inherent in all transformations (except for motion correction transformations which were performed with a trilinear-sinc interpolation), no additional spatial smoothing was performed on the data. MVPA was performed in each subject's native AC-PC space.

For each participant, functional data from each session were screened for motion and/or magnet artifacts by examining the time-course movies and the motion plots created with the motion correction algorithms. None of the runs revealed head motion that exceeded 1.5 mm translation or 1.5° rotation. In Study 1 and 2, error trials—trials in which the participant fumbled with the object (1 trials, 1 participant), contaminated the Plan epoch data by slightly moving their limb (3 trials, 2 participants), or the experimenter replaced the incorrect object (1 trial, 1 participant)—were identified off-line from the videos recorded during the session and were excluded from analysis by assigning these trials predictors of no interest. This very low error rate likely reflects the fact that the task was quite simple (i.e., grasping, lifting, and replacing the object) and that subjects were very well-trained on the delayed timing of the movement task before entering the scanner (through rigorous behavioural testing, see below).

Regions of Interest (ROI)

To localize ROIs for MVPA we used a general linear model (GLM) with predictors created from boxcar functions convolved with the Boynton [S20] hemodynamic response function (HRF). For each trial in Study 1, a boxcar function was aligned to the onset of each phase of the trial, with a height dependent upon the duration of each phase: i) 3-6 volumes for the Plan epoch (due to jittering of delay duration), ii) 1 volume for the Execute epoch, and iii) 7 volumes for the Interaction phase (note that Interaction phase data was not analyzed). For the localizer and object mapping scans, a boxcar function was aligned to the onset of each stimulus block with its duration dependent on stimulus block length. In Study 1 the ITI was excluded from the model, therefore all regression coefficients (betas) were defined relative to the baseline activity during the ITI. In the localizer and object mapping experiments, the Baseline/Fixation epochs were excluded from the model and thus served as baseline in the GLM. For all data, the time-course for each voxel was converted to percent signal change before applying the GLM.

Somatomotor ROIs

To localize the specific *a priori* somatomotor areas in each subject in which to implement MVPA, for each subject, using the Study 1 data, we contrasted activity for movement execution vs. planning (collapsed across heavy and light objects): [Execute(Heavy + Light) > Plan(Heavy + Light)]. The resulting statistical map of all positively active voxels in each subject ($t = 3$, $p < 0.005$, each subject's activation map was cluster threshold corrected, $p < 0.05$) was then used to define three somatomotor ROIs (SSc, M1, and PMd) within the left (contralateral) hemisphere. SSc was chosen to act as a sensory control region (i.e., known to respond to transient stimuli, like sensory events, but not expected to participate in planning-related processes). The voxels included in each ROI were based on all significant contiguous activity within a $(15 \text{ mm})^3 = 3375 \text{ mm}^3$ cube centered on the peak voxel of activity within pre-defined anatomical landmarks (see *ROI selection* below for criteria). These ROI sizes were chosen as it not only allowed the inclusion of several functional voxels for pattern classification (an important consideration), but also ensured that adjacent ROIs did not overlap (for the average number of functional voxels

selected across the 13 subjects, see Table 1). Critically, given the orthogonal contrast employed to select these somatomotor areas (i.e., Execute > Plan, collapsed across conditions), their activity is not directionally biased to show any plan- or execute-related activity pattern differences *between* the heavy versus light object conditions.

Somatomotor ROI selection criterion: Somatosensory cortex (SSc) was defined by selecting voxels encompassing the post-central gyrus and PCS, medial and anterior to aIPS [S9]. Motor cortex (M1) was defined by selecting voxels around the ‘hand knob’ landmark in the central sulcus [S21]. Dorsal premotor (PMd) cortex was defined by selecting voxels at the junction of the pre-central sulcus (PreCS) and superior frontal sulcus (SFS) [S22]. See Table S1 for details about ROI sizes, and Figure S3a for representative locations in a single subject.

To ensure that our decoding accuracies could not result from spurious factors (e.g., task-correlated head or arm movements), we further tested the performance of our classifiers in ROIs where no statistically significant classification should be possible: the ventricles and outside the brain. To select these ROIs we further reduced our statistical threshold (after specifying the [Execute > Plan] network within each subject) down to $t=0$, $p=1$ and selected all activation within 3375 mm^3 centered on consistent points 1) within each subject’s left and right ventricles and, 2) at locations situated just outside the skull of the right and left hemispheres, in the AC-PC plane, directly in line with the posterior commissure. Importantly, pattern classification in these non-brain control ROIs was not statistically significant (data not shown).

Ventral Stream (OTC) ROIs

For each individual subject, each of OTC ROIs was defined based on the peak voxel of a particular contrast (or conjunction) from the localizer experiment and constrained by the anatomical location expected from previous reports (see *Selection criteria* below). Voxelwise and cluster thresholds, selection procedures, and ROI volume constraints were the same as for the somatomotor ROIs.

OTC ROI selection criterion: Object-sensitive activity (LO and pFs) was localized using the object-sensitive localizer based on the contrast of Objects > phase-scrambled objects. Left and right LO was defined around the peak voxel of activity near the lateral occipital sulcus [S23-25]. Left and right pFs was defined around the peak voxel of activity in the posterior aspect of the fusiform gyrus, extending into the occipitotemporal sulcus [S24, S25]. Object texture-sensitive activity was localized using the texture-sensitive localizer by identifying regions in the collateral sulcus and parahippocampal gyrus as well as lateral occipital cortex in both the left and right hemispheres [see S13] based on the conjunction contrast of Ensembles > phase-scrambled versions of these images AND Textures > phase-scrambled versions of these images [Note that we define a conjunction contrast as a Boolean AND, such that for any one voxel to be flagged as significant, it must show a significant difference for each of the constituent contrasts]. See Tables S1 and S2 for details about ROI sizes and Fig. S3B for representative locations on a single subject’s brain.

Visual Cortex Control ROIs

Following the delineation at the single subject level of retinotopic regions V1/V2 using standard procedures [S18] we conducted a voxel-by-voxel conventional amplitude analysis to identify the

sub-region that corresponded to the object-defined area within V1 and V2 for both the Bottom (located dorsal to the calcarine sulcus) and Top (located ventral to the calcarine sulcus) object positions. Voxelwise and cluster thresholds and selection procedures were the same as above with the exception that the activity up to $(10 \text{ mm})^3 = 1000 \text{ mm}^3$ around the voxel peaks were selected [note that these smaller cluster sizes were chosen to avoid the selection of voxels 1) outside of V1 and V2 and, 2) corresponding to the opposite hemi-field (i.e., below the calcarine in the case of the Bottom position object and above the calcarine in the case of the Top position object)]. The Bottom object V1/V2 retinotopic representation was defined using the object-mapping localizer data by the contrast of [Bottom > ITI] and the Top object V1/V2 retinotopic representation was defined by the contrast of [Top > ITI].

Multivariate pattern analysis (MVPA)

Support Vector Machine Classifiers:

MVPA was performed with a combination of in-house software (using Matlab) and the Princeton MVPA Toolbox for Matlab (<http://code.google.com/p/princeton-mvpa-toolbox/>) using a Support Vector Machines (SVM) binary classifier (libSVM, <http://www.csie.ntu.edu.tw/~cjlin/libsvm/>). The SVM model used a linear kernel function and a constant cost parameter, $C=1$ ([congruent with many other fMRI studies, S26, S27-30]) to compute a hyperplane that best separated the trial responses. We used a “leave-one-run-out” N-fold cross-validation to test the accuracy of the SVM classifiers and then averaged across the N-iterations in order to produce a representative classification accuracy measure for each experiment, subject, ROI, trial epoch, and pair-wise discrimination [S31]. We statistically assessed decoding significance across participants using a two-tailed t-test versus 50% chance decoding. A false discovery rate (FDR) correction of $q \leq 0.05$ was applied based on the number of ROIs considered in our analyses [S32].

Inputs to Classifier:

To prepare the data for voxel pattern classification, the percent signal change was computed from the time-course activity at a time point(s) of interest with respect to the time-course at a common baseline, for all voxels in the ROI. The baseline window was defined as a run-based average of volume -1, a time point prior to onset of each trial and avoiding contamination from responses of the previous trial. For the Plan epoch—the time points of critical interest—we extracted the average of the final two volumes prior to the subject hearing the auditory cue to initiate a movement. For the Execute epoch time points, we extracted the average of volumes 4-5 (with respect to onset of the Execute epoch), time points generally corresponding to the peak (and time point following the peak) of the transient execution response, which follows from the subject’s action. These time points extracted for pattern classification directly follows from our previous work [S8-12]. Following the extraction of each trial's percent signal change activity, these values were rescaled between -1 and +1 across all trials for each individual voxel within an ROI [S33].

Behavioural Control Experiments

Overview of Procedures

All subjects participated in two additional behavioural testing sessions. In the first session, subjects’ eye fixations and the forces they applied to objects for lifting were measured as they completed the Study 1 task. This testing session was used for participant screening (as it was

performed before the MRI experiments) and to determine, from an analysis of their behaviour, whether they were i) maintaining in memory over the delay periods of each event-related trial (i.e., Plan epoch) the weight of the object to be lifted and, ii) able to reliably maintain fixation over the duration of an MRI scan. Each subject completed 8 experimental runs, identical to those performed in the scanner.

In the second session, in addition to monitoring participant eye fixations and object lifting forces for the Study 2 task, we examined the possibility that the successful decoding of weight information in LOC for Study 1, rather than reflecting sensorimotor memory for object weight, might instead be accounted for by subtle visual differences between the two objects used. Although our decoding results from V1/V2 suggest this alternative explanation to be highly unlikely, we additionally tested for this possibility at the behavioural level by examining 1) whether subjects could adjust their lifting forces in accordance with changes in the object being presented (i.e., requiring subjects to visually detect when the object has changed from trial-to-trial) and 2) whether, when explicitly made part of the task, subjects could visually distinguish the two objects in a 1-back 'same' or 'different' perceptual discrimination paradigm (see below for details).

This second behavioural testing session was composed of several parts. In the first part, subjects completed tasks that were identical to those performed in the scanner in Study 2 and in the following order: 1) they performed alternated lifting, 15 times each, of the two Study 2 objects with the stereotypical object texture-weight mapping (metal heavy object, wood light object), familiarizing them with the two objects, 2) they completed one experimental run with those same objects, 3) they performed alternated lifting, 15 times each, of the two Study 2 objects with the inverted object texture-weight mapping (metal light object, wood heavy object), familiarizing them with the new object texture-weight relationships, and 4) they completed one experimental run with those same inverted objects. The aim of the first part of this behavioural testing session was to demonstrate that subjects i) quickly learned the weights of the inverted texture-weight objects, ii) had no difficulty maintaining in memory over the delay periods (i.e., Plan epoch) of each event-related trial the weight of the object to be lifted and, iii) were able to reliably maintain fixation over the duration of the task.

In the second part of this testing session, subjects completed two separate blocks of 70 trials (140 total) in which they lifted a centrally located object every ~10-12 seconds (the objects lifted were the same objects as those used in Study 1). In between trials, an opaque shutter screen, located between the participant and object location, was closed by the experimenter, obscuring vision of the workspace. During this time, the object was either changed by the experimenter (from a heavy to light object or vice versa) or simply lifted and replaced, according to a semi-randomized schedule such that the object was changed by the experimenter every 7 ± 2 trials. [Note that consistent actions by the experimenter (i.e., changing or replacing the object) in between trials made it impossible for the subjects to use other cues for predicting when in fact the object was changed]. Once the object was correctly positioned by the experimenter for the upcoming trial, the shutter screen was opened and the participant was required to grasp and lift the object once cued by an auditory 'beep' (this 'beep' cue was controlled by the experimenter via keyboard, ensuring that subject's never received this lift cue prior to the shutter screen being open). While the shutter screen was open, subjects were required to maintain fixation to a centrally located dot

displayed on a computer monitor; the monitor was located behind the force sensor platform upon which the object was placed and the fixation dot was displayed directly above the object. While the shutter screen was closed, subjects were required to maintain fixation on a dot (small red sticker) centered on the shutter screen itself (at approximately the same horizontal and vertical location that the fixation dot would appear on the monitor when the shutter screen was open). The aim of this behavioural experiment was to determine whether subjects could exploit any subtle visual differences between the two Study 1 objects so as to reliably adjust their lifting forces in accordance with the experimenter changes in object weight. Post-experiment verbal reports indicated that participants could not predict on which particular trials the object was changed by the experimenter (with the exception that they did notice that once changed by the experimenter (e.g., from light to heavy weight), the object would not again be changed within the following 2-3 trials).

In the third and final part of this behavioural testing session, subjects completed 101 trials in which they made perceptual judgments, via key press responses with their right and left hands, whether the object presented on the current trial was the same or different, respectively, than the object presented on the previous trial (i.e., 1-back perceptual discrimination task; note that participant responses on the first trial of this task were not analyzed). The objects used in this experiment were the same objects as those used in Study 1. The general task and apparatus was the same as that of the second part of the testing session (see paragraph above) with the exception that the objects were changed by the experimenter according to a fully randomized schedule and that subjects indicated their perceptual reports (same or different object) via two hand-held button-response devices. The aim of this behavioural experiment was to determine whether subjects could exploit any subtle visual differences in the two Study 1 objects to reliably discriminate object identity from trial to trial.

Setup and Analysis

Object lifting trials

In each object lifting trial, participants lifted an object from a tabletop platform instrumented with force sensors (Nano 17 F/T sensors; ATI Industrial Automation, Garner, NC) and then replaced the object in the same location. The platform contained two sensors that were capped with flat circular disks with a diameter of 3 cm. These force sensors allowed for the precise measurement of the vertical load force applied to the object during lifting up until the point that the object was lifted off the disk. Prior to beginning the experiments, participants received both verbal instructions and a demonstration by the experimenter as to how to perform the lifting actions. Following the first behavioural experiment, subjects recruited to participate in the fMRI experiments were then instructed to use this exact same procedure for lifting objects in the MRI scanner.

Vertical forces from the force sensors were sampled at 1000 Hz. The raw force signals were low-pass filtered using a 4th order, zero-phase lag Butterworth filter with a cutoff frequency of 14 Hz. The processed signal was then differentiated with respect to time using a 1st order central difference equation to obtain the rate of change in load force, or load-force rate, which represents the rate of change of load force applied by the hand to the object. For each lift, we determined the first peak in load-force rate during the lift. People tend to lift objects of varying weight in about the same amount of time. To accomplish this consistency, they scale the load force rate,

before object lift-off, to the expected weight of the object. When the instructed lift height is small (e.g., ~2cm as in the current study), people typically reduce the load-force rate so that it approaches zero at the expected lift-off time. Thus, the peak rate of change of load force, which occurs prior to lift-off, provides an index of predicted weight [S1, S34, S35].

Eye-tracking

An infrared video-based eye-tracking system (ETL 500 pupil/corneal tracking system, ISCAN Inc. Burlington, MA, USA), mounted below a headband, recorded the gaze position of the left eye at 240 Hz as participants maintained fixation at a dot displayed on a computer monitor (1024 x 768; 60 Hz refresh rate) located directly behind the tabletop platform containing the force sensors (and positioned at an average across-subjects height above the object of ~9.45° visual angle). Gaze was calibrated using a two-step procedure: an initial 5-point calibration using ISCAN's Line-of-Sight Plane Intersection Software followed by a 25-point calibration routine (see Johansson et al. 2001 for details). Calibration points (4 mm-diameter circles) were shown on the computer monitor where the fixation point was projected and distributed over a region that incorporated the hand start location and potential object positions (i.e., location of the two force sensors). The ISCAN calibration converted raw gaze signals into pixels from the line-of-sight camera and the 25-point calibration converted pixels (i.e., the output of the ISCAN calibration) into the coordinates of the computer monitor. Gaze was calibrated at the start of the experiment and was checked following each block of trials so that, if necessary, gaze could be re-calibrated before starting a new test block.

References:

- S1. Flanagan, J.R., Bittner, J.P., and Johansson, R.S. (2008). Experience can change distinct size-weight priors engaged in lifting objects and judging their weights. *Current biology* : *CB 18*, 1742-1747.
- S2. Oldfield, R.C. (1971). The assessment and analysis of Handedness: the Edinburgh inventory. *Neuropsychologia* *9*, 97-113.
- S3. Chapman, C.S., Gallivan, J.P., Culham, J.C., and Goodale, M.A. (2011). Mental Blocks: fMRI reveals top-down modulation of early visual cortex when planning a grasp movement that is interfered with by an obstacle. *Neuropsychologia* *49*, 1703-1717.
- S4. Curtis, C.E., Rao, V.Y., and D'Esposito, M. (2004). Maintenance of spatial and motor codes during oculomotor delayed response tasks. *The Journal of neuroscience : the official journal of the Society for Neuroscience* *24*, 3944-3952.
- S5. Beurze, S.M., de Lange, F.P., Toni, I., and Medendorp, W.P. (2007). Integration of target and effector information in the human brain during reach planning. *Journal of neurophysiology* *97*, 188-199.
- S6. Pertzov, Y., Avidan, G., and Zohary, E. (2011). Multiple reference frames for saccadic planning in the human parietal cortex. *The Journal of neuroscience : the official journal of the Society for Neuroscience* *31*, 1059-1068.
- S7. Beurze, S.M., de Lange, F.P., Toni, I., and Medendorp, W.P. (2009). Spatial and effector processing in the human parietofrontal network for reaches and saccades. *Journal of neurophysiology* *101*, 3053-3062.
- S8. Gallivan, J.P., McLean, D.A., Smith, F.W., and Culham, J.C. (2011). Decoding effector-dependent and effector-independent movement intentions from human parieto-frontal brain activity. *Journal of Neuroscience* *31*, 17149-17168.
- S9. Gallivan, J.P., McLean, D.A., Valyear, K.F., Pettypiece, C.E., and Culham, J.C. (2011). Decoding action intentions from preparatory brain activity in human parieto-frontal networks. *Journal of Neuroscience* *31*, 9599-9610.
- S10. Gallivan, J.P., McLean, D.A., Valyear, K.F., and Culham, J.C. (2013). Decoding the neural mechanisms of human tool use. *eLife* *2*, e00425.
- S11. Gallivan, J.P., McLean, D.A., Flanagan, J.R., and Culham, J.C. (2013). Where one hand meets the other: limb-specific and action-dependent movement plans decoded from preparatory signals in single human frontoparietal brain areas. *The Journal of neuroscience : the official journal of the Society for Neuroscience* *33*, 1991-2008.
- S12. Gallivan, J.P., Chapman, C.S., McLean, D.A., Flanagan, J.R., and Culham, J.C. (2013). Activity patterns in the category-selective occipitotemporal cortex predict upcoming motor actions. *The European journal of neuroscience* *38*, 2408-2424.
- S13. Cant, J.S., and Xu, Y. (2012). Object ensemble processing in human anterior-medial ventral visual cortex. *Journal of Neuroscience* *32*, 7685-7700.
- S14. Arcaro, M.J., Pinsk, M.A., Li, X., and Kastner, S. (2011). Visuotopic organization of macaque posterior parietal cortex: a functional magnetic resonance imaging study. *The Journal of neuroscience : the official journal of the Society for Neuroscience* *31*, 2064-2078.

- S15. Arcaro, M.J., McMains, S.A., Singer, B.D., and Kastner, S. (2009). Retinotopic organization of human ventral visual cortex. *The Journal of neuroscience : the official journal of the Society for Neuroscience* 29, 10638-10652.
- S16. Swisher, J.D., Halko, M.A., Merabet, L.B., McMains, S.A., and Somers, D.C. (2007). Visual topography of human intraparietal sulcus. *The Journal of neuroscience : the official journal of the Society for Neuroscience* 27, 5326-5337.
- S17. DeYoe, E.A., Carman, G.J., Bandettini, P., Glickman, S., Wieser, J., Cox, R., Miller, D., and Neitz, J. (1996). Mapping striate and extrastriate visual areas in human cerebral cortex. *Proceedings of the National Academy of Sciences of the United States of America* 93, 2382-2386.
- S18. Sereno, M.I., Dale, A.M., Reppas, J.B., Kwong, K.K., Belliveau, J.W., Brady, T.J., Rosen, B.R., and Tootell, R.B. (1995). Borders of multiple visual areas in humans revealed by functional magnetic resonance imaging. *Science* 268, 889-893.
- S19. Engel, S.A., Glover, G.H., and Wandell, B.A. (1997). Retinotopic organization in human visual cortex and the spatial precision of functional MRI. *Cerebral cortex* 7, 181-192.
- S20. Boynton, G.M., Engel, S.A., Glover, G.H., and Heeger, D.J. (1996). Linear systems analysis of functional magnetic resonance imaging in human V1. *The Journal of neuroscience : the official journal of the Society for Neuroscience* 16, 4207-4221.
- S21. Yousry, T.A., Schmid, U.D., Alkadhi, H., Schmidt, D., Peraud, A., Buettner, A., and Winkler, P. (1997). Localization of the motor hand area to a knob on the precentral gyrus. A new landmark. *Brain : a journal of neurology* 120, 141-157.
- S22. Picard, N., and Strick, P.L. (2001). Imaging the premotor areas. *Current opinion in neurobiology* 11, 663-672.
- S23. Malach, R., Reppas, J.B., Benson, R.R., Kwong, K.K., Jiang, H., Kennedy, W.A., Ledden, P.J., Brady, T.J., Rosen, B.R., and Tootell, R.B. (1995). Object-related activity revealed by functional magnetic resonance imaging in human occipital cortex. *Proceedings of the National Academy of Sciences of the United States of America* 92, 8135-8139.
- S24. Grill-Spector, K., Kourtzi, Z., and Kanwisher, N. (2001). The lateral occipital complex and its role in object recognition. *Vision research* 41, 1409-1422.
- S25. Grill-Spector, K., Kushnir, T., Edelman, S., Avidan, G., Itzhak, Y., and Malach, R. (1999). Differential processing of objects under various viewing conditions in the human lateral occipital complex. *Neuron* 24, 187-203.
- S26. Haynes, J.D., Sakai, K., Rees, G., Gilbert, S., Frith, C., and Passingham, R.E. (2007). Reading hidden intentions in the human brain. *Current biology : CB* 17, 323-328.
- S27. Pessoa, L., and Padmala, S. (2007). Decoding near-threshold perception of fear from distributed single-trial brain activation. *Cerebral cortex* 17, 691-701.
- S28. LaConte, S., Anderson, J., Muley, S., Ashe, J., Frutiger, S., Rehm, K., Hansen, L.K., Yacoub, E., Hu, X., Rottenberg, D., et al. (2003). The evaluation of preprocessing choices in single-subject BOLD fMRI using NPAIRS performance metrics. *NeuroImage* 18, 10-27.
- S29. Mourao-Miranda, J., Bokde, A.L., Born, C., Hampel, H., and Stetter, M. (2005). Classifying brain states and determining the discriminating activation patterns: Support Vector Machine on functional MRI data. *NeuroImage* 28, 980-995.

- S30. Mitchell, T.M., Hutchinson, R., Just, M.A., Niculescu, R.S., Pereira, F., and Wang, X. (2003). Classifying instantaneous cognitive states from FMRI data. *AMIA Annu Symp Proc*, 465-469.
- S31. Duda, R.O., Hart, P.E., and Stork, D.G. (2001). *Pattern Classification, Second Edition* Edition, (New York: John Wiley & Sons, Inc.).
- S32. Benjamini, Y., and Hochberg, Y. (1995). Controlling the false discovery rate: a practical and powerful approach to multiple testing. *Journal of the Royal Statistical Society* 57, 289-300.
- S33. Misaki, M., Kim, Y., Bandettini, P.A., and Kriegeskorte, N. (2010). Comparison of multivariate classifiers and response normalizations for pattern-information fMRI. *NeuroImage* 53, 103-118.
- S34. Flanagan, J.R., and Beltzner, M.A. (2000). Independence of perceptual and sensorimotor predictions in the size-weight illusion. *Nature neuroscience* 3, 737-741.
- S35. Johansson, R.S., and Westling, G. (1988). Coordinated isometric muscle commands adequately and erroneously programmed for the weight during lifting task with precision grip. *Experimental brain research. Experimentelle Hirnforschung. Experimentation cerebrale* 71, 59-71.